RESEARCH ARTICLE

Theoretical perspectives on central chemosensitivity: CO_2/H^+-sensitive neurons in the locus coeruleus

Maria C. Quintero[1]*, Robert W. Putnam[2], Juan M. Cordovez[1]*

1 Biomedical Engineering Department, Universidad de Los Andes, Bogotá, Colombia, **2** Department of Neuroscience, Cell Biology, and Physiology, Boonshoft School of Medicine, Wright State University, Dayton, Ohio, United States of America

* mc.quintero144@uniandes.edu.co (MQ); jucordov@uniandes.edu.co (JC)

Abstract

Central chemoreceptors are highly sensitive neurons that respond to changes in pH and CO_2 levels. An increase in CO_2/H^+ typically reflects a rise in the firing rate of these neurons, which stimulates an increase in ventilation. Here, we present an ionic current model that reproduces the basic electrophysiological activity of individual CO_2/H^+-sensitive neurons from the locus coeruleus (LC). We used this model to explore chemoreceptor discharge patterns in response to electrical and chemical stimuli. The modeled neurons showed both stimulus-evoked activity and spontaneous activity under physiological parameters. Neuronal responses to electrical and chemical stimulation showed specific firing patterns of spike frequency adaptation, postinhibitory rebound, and post-stimulation recovery. Conversely, the response to chemical stimulation alone (based on physiological CO_2/H^+ changes), in the absence of external depolarizing stimulation, showed no signs of postinhibitory rebound or post-stimulation recovery, and no depolarizing sag. A sensitivity analysis for the firing-rate response to the different stimuli revealed that the contribution of an applied stimulus current exceeded that of the chemical signals. The firing-rate response increased indefinitely with injected depolarizing current, but reached saturation with chemical stimuli. Our computational model reproduced the regular pacemaker-like spiking pattern, action potential shape, and most of the membrane properties that characterize CO_2/H^+-sensitive neurons from the locus coeruleus. This validates the model and highlights its potential as a tool for studying the cellular mechanisms underlying the altered central chemosensitivity present in a variety of disorders such as sudden infant death syndrome, depression, and anxiety. In addition, the model results suggest that small external electrical signals play a greater role in determining the chemosensitive response to changes in CO_2/H^+ than previously thought. This highlights the importance of considering electrical synaptic transmission in studies of intrinsic chemosensitivity.

Author summary

The sensory mechanism by which changes in CO_2 and H^+ levels are detected in the brain is known as central chemoreception. Altered chemoreception is common to a wide variety of clinical conditions, including sleep apnea, sudden infant death syndrome, hyperventilation, depression, anxiety and asthma. In addition, CO_2/H^+-sensitive neurons are present in some regions of the brain that have been identified as drug targets for the treatment of anxiety and panic disorders. We are interested in understanding the cellular mechanisms that determine and modulate the behavior of these neurons. We previously investigated possible mechanisms underlying their behavior in rats to elucidate whether they respond to changes in intracellular or extracellular pH, CO_2, or a combination of these stimuli. To study the roles that signals and ion channel targets play in individual neurons we develop mathematical models that simulate their electrochemical behavior and their responses to hypercapnic and/or acidotic stimuli. Nowadays, we are focused on using computational tools to explore the firing pattern of such neurons in response to chemical (CO_2/H^+) and electrical (synaptic) stimulation. Our results reveal significant effects of electrical stimulation on the responses of brainstem neurons and highlight the importance of considering synaptic transmission in experimental studies of chemosensitivity.

Introduction

Central chemoreception is a neuronal sensory mechanism by which changes in CO_2 and H^+ levels in the brain are detected [1–3]. It occurs in specialized CO_2/H^+-sensitive centers in the brainstem that are involved in the neuronal network that regulates autonomic ventilation [4–10]. Regular ventilatory movements are controlled by respiratory neurons in the brainstem, which generate an appropriate respiratory rhythm and control the motor neurons that innervate the respiratory muscles [11–14]. Even small alterations in CO_2/H^+ levels in the blood and/or cerebrospinal fluid cause changes in ventilation. Brainstem neurons are considered the main sensory elements in the homeostatic regulation of respiratory gases [15,16], and when these neurons are exposed to elevated CO_2/H^+ (hypercapnia and/or acidosis), there is a noticeable increase in their firing rate. This change in firing rate can be triggered by several signaling pathways alone or in combination, such as a decrease in intracellular or external pH [17,18], an increase in intracellular HCO_3^- [19] and/or a direct increase in CO_2 [20].

The changes in firing rate of neurons from chemosensitive regions have been investigated under conditions of hypercapnic acidosis (HA) in some areas of the brainstem, such as the retrotrapezoid nucleus [21], nucleus tractus solitarii [22,23], locus coeruleus [24–26] and the medullary *raphe* [27]. It is often assumed that these neurons are intrinsically responsive to changes of CO_2, which means that they not simply respond to altered synaptic input from other chemosensitive neurons. In particular, neurons from LC have been demonstrated to be responsive when exposed to altered levels of CO_2 in the presence of synaptic block media. However, it remains unclear whether their firing-rate response to increased levels of CO_2/H^+ can be completely attributed to intrinsic mechanisms of individual neurons or if the response is mediated in part by unnoticed inputs from chemical synapses or gap junctions [18,23,28].

Moreover, since there have been postulated a growing number of signals implicated in the chemosensitive response of individual neurons from the LC region [17–20], the knowledge about the various signals, both excitatory and inhibitory, is getting so complex that our ability to understand the interactions between these differing components needs to be aided by mathematical and computational approaches. In particular, a single-cell neuron model is required

to elucidate the effect of individual signals and their interaction on the chemosensitive response of individual neurons. Such an approach would help to elucidate whether their spike patterns and discharge frequencies are significantly affected by individual signals, by the combined effect of different stimuli, or by a contribution of small external inputs.

Experimental evidence suggests that neurons from different chemosensitive regions are similar in their basal discharge frequencies and spiking patterns in response to current injection [27–29]. On the other hand, some mathematical models of the Hodgkin–Huxley type have been used to explore electrical behavior and neurophysiological characteristics in neurons from several regions of the brainstem [30–35]. For example, some well-known phenomena associated with the neuronal electrical behavior such as spike frequency adaptation (SFA), post-stimulation recovery or delayed excitation, and postinhibitory rebound (PIR) have been related to specific ionic current mechanisms in medullary neurons [31,32] and in some cases these phenomena have been used to classify neurons by their electrophysiological behavior in response to electrical stimuli [30]. However none of these models examined specific electrical behaviors and related ionic mechanisms in individual neurons from chemosensitive regions, neither they have explored their intrinsic properties associated with their response to hypercapnic or acidotic stimuli.

The chemosensitive response of these neurons to acidotic stimuli affects respiratory, arousal, emotional and memory circuits. It is therefore important to study the responses of individual neurons to changes in pH and CO_2, and to understand the cellular signaling mechanisms that govern autonomic and respiratory responses to such changes. This will, in turn, contribute to our understanding of the etiology of disorders with respiratory manifestations such as sudden infant death syndrome [12], sleep apnea [36], panic attacks [37–40], or Rett syndrome [41].

Given the potential wide-ranging impact of understanding the cellular mechanisms governing CO_2/H^+ sensitivity in neurons from chemosensitive regions, it is important to develop a model that faithfully replicates the effect of CO_2/H^+ on the activity of individual chemoreceptors. In the current study we propose a single cell model framework for a CO_2/H^+-sensitive neuron that mimics the general electrophysiological discharge patterns of locus coeruleus neurons at rest, as well as in response to electrical and chemical stimuli. Our main goal in this study was to investigate 1) intrinsic neuronal activity in absence of all possible external input from electrical and chemical stimuli; 2) the effects of excitatory and inhibitory stimuli on neuronal activity; and 3) the role that individual signals and chemical stimuli may play in the chemosensitive response.

Results

In general, the model yielded regular activity at slow frequencies with the application of a small depolarizing current of 10–80 pA within a wide range of parameters. The method applied to integrate the system is also robust in the sense of converging to a bifurcation from resting activity to spiking over a wide range of starting parameter values.

For the set of parameter values used in this study, both electrical and some chemical signals play the role of bifurcation parameters. In particular, the equilibrium of the system loses stability with relatively high hyperpolarizing stimuli, be it an applied current of magnitude higher than 0.002 nA, an increase of the intracellular pH to higher values than 7.5, or an extracellular pH exceeding 7.58. Thus, spiking at arbitrarily low frequencies is only possible within a smaller range of parameters relative to the wide range at which higher frequencies are possible. This change in the state of the system from spiking to resting activity comes presumably from the

Table 1. Experimental and calculated values for electrophysiological properties.

	Basic characteristics of action potential			Average chemosensitive response	
	Thresh.(mV)	AHP (mV)	Amplitude (mV)	Initial FR (Hz)	% Change in FR (HA)
Exp.	-48.5 ± 6.4	17.5 ± 2.5	76.3 ± 5.7	1.75 ± 1.25	119.5
Model	-50.3 ± 4.6	16.7 ± 2.2	70 ± 4.5	1.43 ± 2.19	99.3

Average values obtained with the neuron model in accordance with experimental data (Exp.) from spontaneous action potentials of LC chemosensitive neurons. Threshold, afterhyperpolarization (AHP), amplitude, initial firing rate (FR) and the percentage increase in FR at hypercapnic acidosis (HA). Experimental values were averaged with those taken from [18,29,43].

https://doi.org/10.1371/journal.pcbi.1005853.t001

ability of these parameters to move the dynamical system away from an Andronov-Hopf bifurcation, which prevents the model to oscillate at arbitrarily low frequencies.

Validation of the model

The model was used to examine the typical firing properties of individual neurons that are common among various chemosensitive regions of the brainstem [42,43]. To assess intrinsic activity in absence of all possible input from electrical and chemical stimuli, the stimulus current (I_s) was initially set to zero and CO_2/H^+ levels established at normocapnic conditions. Simulations resulted in spontaneous regular pacemaker-like activity characteristic of chemosensory neurons [44–48]. Some other characteristics, such as membrane properties and action potential shapes, were also within the range observed for these chemosensitive neurons at normal and hypercapnic conditions (Table 1).

In particular, simulations were run to predict some of the more important firing properties of individual chemosensitive neurons from the LC and to validate the model with intracellular recordings. As can be seen in Fig 1 the model results in spontaneous action potentials with a regular spiking pattern and with membrane properties (action potential shape, AHP phase, and frequency) similar to those observed in LC neurons.

Neurocomputational aspects

To simulate the basic electrochemical behavior of a chemosensitive neuron, we subjected the model to electrical (from external stimulus current) and chemical (changes in CO_2/H^+)
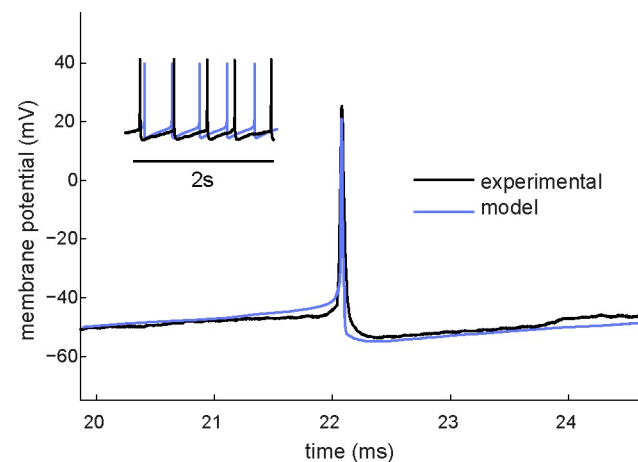

Fig 1. Comparison of experimental and model-generated data. LC neuron (black) and model-generated action potential waveforms (blue) were recorded during normal spontaneous activity. The model is capable of reproducing a similar pattern of AHP existent throughout the entire interspike interval observed in LC neurons.
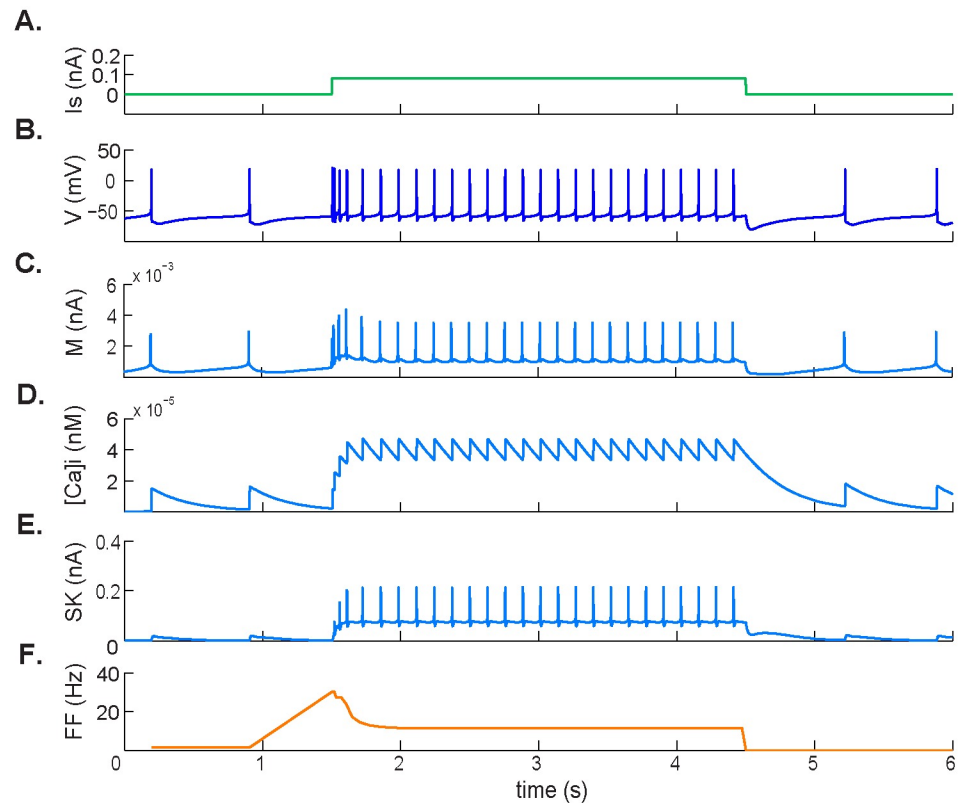
https://doi.org/10.1371/journal.pcbi.1005853.g001

Fig 2. Spike frequency adaptation response to applied depolarizing current. A. Applied 0.1 nA depolarizing pulse. **B.** Simulated membrane potential during the pulse. **C.** M-type potassium current dynamics showing an increase in response to initial depolarization followed by a new, elevated steady state during stimulation. **D.** Intracellular calcium concentration $[Ca^{2+}]_i$. **E.** Calcium-activated SK-type potassium current. $[Ca^{2+}]_i$ and SK-type potassium current are both involved in the change in firing rate during depolarizing stimuli. **F.** Firing frequency.

https://doi.org/10.1371/journal.pcbi.1005853.g002

stimuli. Neuronal responses were distinguished by specific firing pattern phenomena, namely spike frequency adaptation, postinhibitory rebound, and post-stimulation recovery.

Spike frequency adaptation. The model-generated membrane potential during the application of a depolarizing current pulse is shown in Fig 2. In agreement with [29], depolarization within the range between 0.06nA and 0.21nA caused an initial increase in the firing rate, which adapted to a lower steady-state level. In particular, when applying a depolarizing current of 0.1 nA in normocapnia, we obtained a peak frequency of 30 Hz that adapted to a steady-state value of 8 Hz, resulting in an SFA ratio of 3.75 (Fig 2F).

Fig 3 shows the cell subjected only to an excitatory chemical stimulus. In Fig 3A and 3B, the simulated membrane potential is shown during an increase in CO_2 level from 5% to 15% (hypercapnic acidosis) and the firing frequency adaptation can be seen in Fig 3E. With relatively low values for peak and steady-state frequency (3.5 Hz and 2.8 Hz, respectively), it resulted in an SFA ratio of 1.25.

Postinhibitory rebound. Although this behavior has not been fully reported in LC neurons as far as we know, simulations resulted in spiking following a release from hyperpolarization, typical of some respiratory related neurons. Fig 4 shows the dynamic response of the membrane potential and the currents that were most affected when an inhibitory stimulus was released and followed by the application of a depolarizing current. This resulted in an increase
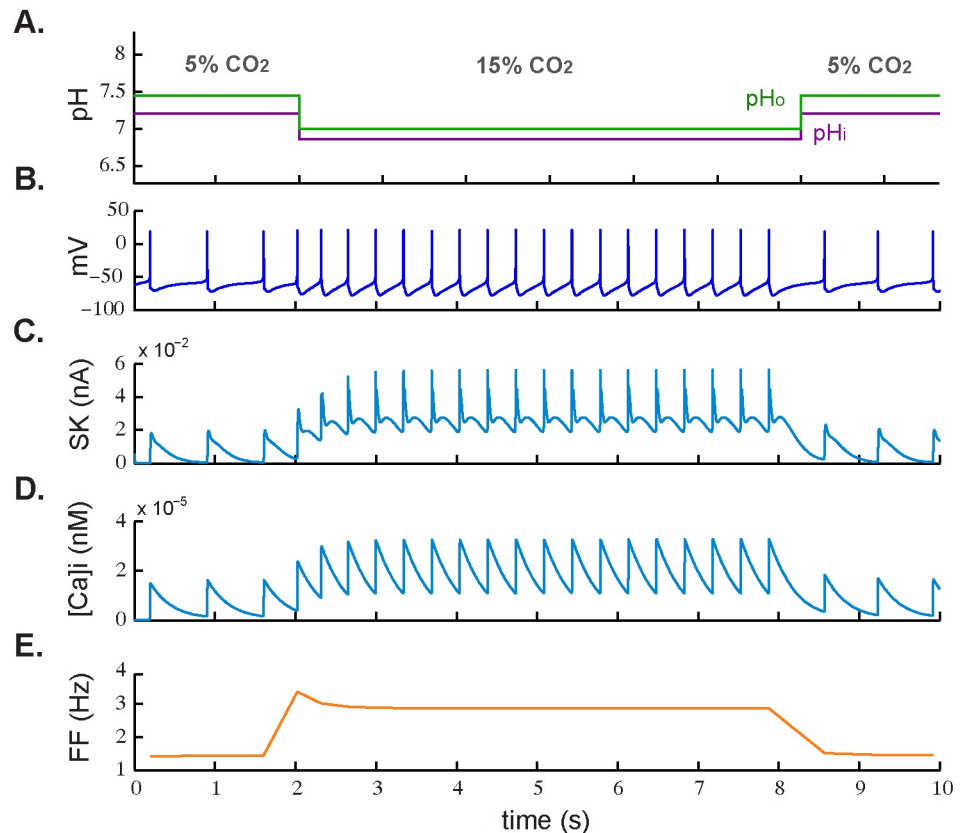
Fig 3. Spike frequency adaptation response to excitatory chemical stimulus. A. Simulated application of normocapnic (5% CO_2) and hypercapnic acidotic (15% CO_2) stimuli. **B.** Corresponding simulated membrane potential. **C.** Dynamic response of calcium-activated SK-type potassium current. **D.** Dynamic response of intracellular calcium concentration ($[Ca^{2+}]_i$). **E.** Firing frequency during CO_2 level change.

https://doi.org/10.1371/journal.pcbi.1005853.g003

in T-type current, which depolarized the membrane and promoted accumulation of intracellular calcium. There was also an increase in A-type current (Fig 4B) that limited the rebound spiking frequency.

Post-stimulation recovery. This passive electrophysiological property is characteristic of LC neurons and has been observed upon termination of hyperpolarizing currents around 0.5nA immediately followed by a depolarizing current of 0.2nA [29]. Simulations at the above range of hyperpolarizing and depolarizing currents and the resulting behavior is illustrated in Fig 4. Fig 4C shows the restoration of baseline membrane potential after the rebound that appeared due to the depolarizing pulse. Here, the electrical stimulus caused an increase in the average level of $[Ca^{2+}]_i$ and, upon termination of the rebound, the level of $[Ca^{2+}]_i$ started to decay. Once resting levels of $[Ca^{2+}]_i$ were restored, spiking resumed at an increased steady-state rate.

Chemosensitive behavior

To simulate the basic chemosensitive behavior of a locus coeruleus neuron, we subjected the model to different levels of CO_2/H^+. As expected, neuronal responses were characterized by increased firing frequencies when related parameters where established to simulate hypercapnic and acidotic conditions in accordance with previous experiments in LC [49]. As illustrated
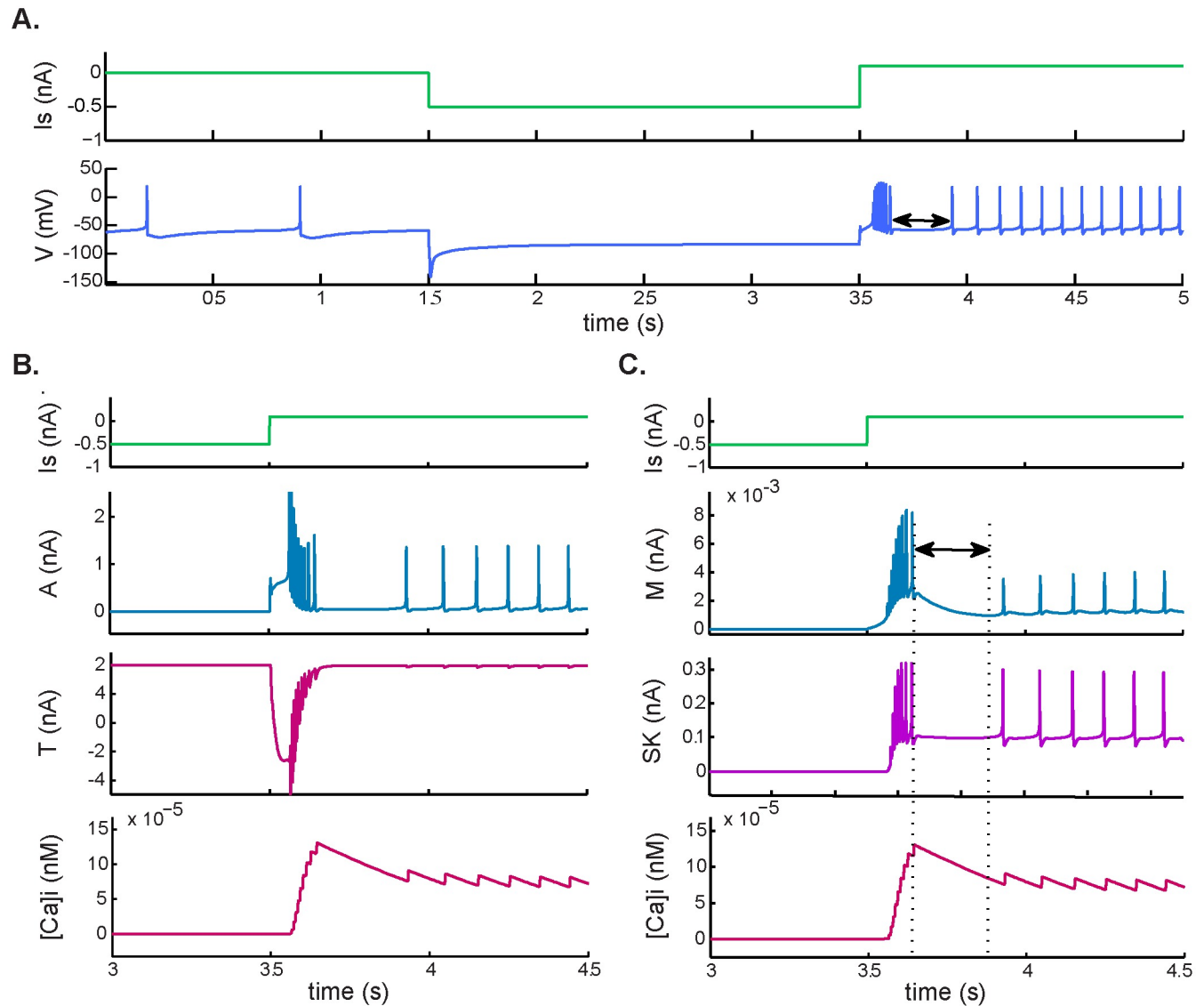
Fig 4. Postinhibitory rebound and post-stimulation recovery. Response to a hyperpolarizing pulse of −0.5 nA followed by a depolarizing pulse of 0.6 nA. **A.** Simulated membrane potential during current application. **B.** Postinhibitory rebound, involving an increase in A-type potassium and T-type calcium currents and an increase in intracellular calcium ($[Ca^{2+}]_i$). **C.** Post-stimulation recovery after postinhibitory rebound. This behavior was associated with accumulation of $[Ca^{2+}]_i$ and increased M-type and SK potassium currents.

https://doi.org/10.1371/journal.pcbi.1005853.g004

in Fig 5 the predicted changes in frequency resulting from the chemosensitive response in the model are in agreement with intracellular recordings of LC neurons.

We next investigated the effects of excitatory and inhibitory chemical stimuli (i.e. hypercapnic acidosis followed by hypocapnic alkalosis) on the tonic firing rate (Fig 6). In contrast with the electrical behavior in response to depolarizing and hyperpolarizing external stimuli, there was no evidence of postinhibitory rebound or post-stimulation recovery, and no depolarizing sag, when the stimulation was based on physiological CO_2/H^+ changes.

Here, the neuronal response to inhibition by hypocapnic acidosis (2.5% CO_2) resulted in a hyperpolarization of the membrane potential that prevented the neuron from firing. This hyperpolarizing effect was released by subsequent hypercapnic acidosis (15% CO_2), which
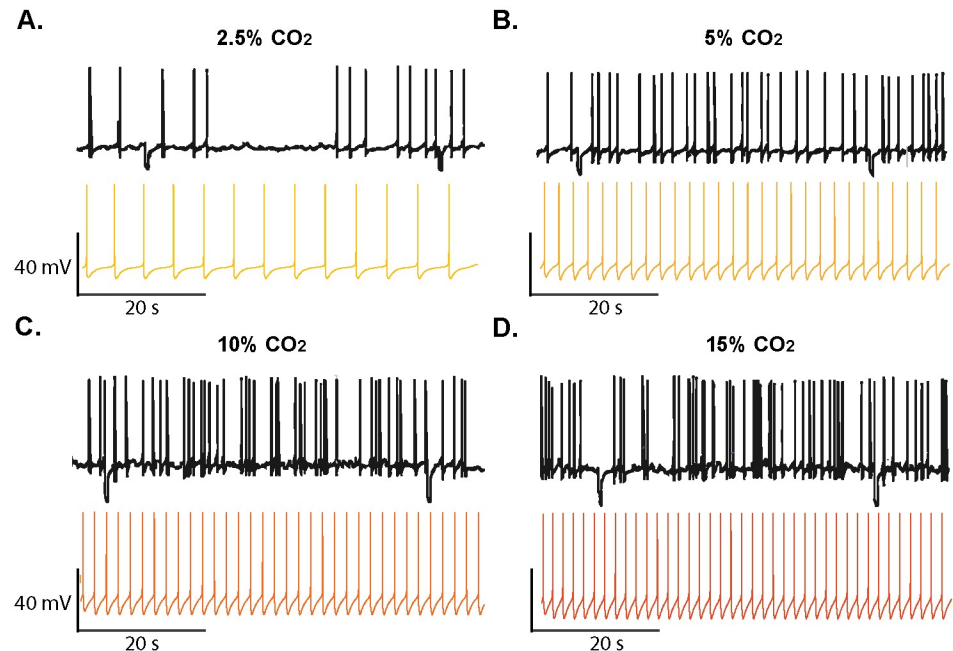
Fig 5. Comparison of simulated chemosensitive behavior and intracellular recordings. Effect of hypocapnia and hypercapnia on the spontaneous firing rate in locus coeruleus (LC) neurons from rats. **A.** Hypocapnic alkalosis (2.5% CO2, pH_o = 7.55, pH_i = 7.3). **B.** Normocapnia (5% CO2, pH_o = 7.45, pH_i = 7.23); **C.** Hypercapnia (10% CO2, pH_o = 7.15, pH_i = 7.4); **D.** Hypercapnic acidosis (15%CO2, pH_o = 7, pH_i = 6.96). Traces of membrane potential (Vm) vs. time showing action potential frequency from experimental data (black) and model-generated data (colored) for different conditions. Experimental traces were redrawn from data from Li and Putnam (2013) [45].

https://doi.org/10.1371/journal.pcbi.1005853.g005

made the neuron fire at higher frequencies and caused a new, elevated tonic firing rate compared with normocapnic conditions (5% CO_2). There was no evidence for postinhibitory rebound before hypocapnic inhibition, consistent with a lower accumulation of $[Ca^{2+}]_i$ and inhibition of the L-type current during hypocapnic conditions.

Effect of individual signals and chemical stimuli

To understand the effect of individual signals, whether electrical or chemical, on the activity of the neuron, we calculated the sensitivity of the firing-rate response to each signal (Table 2). A sensitivity index (SI) was thus defined as the percentage of control firing rate to which the activity increases or decreases in response to a change in each signal (Δs):

$$SI = \frac{|FR_s - FR_c|}{FR_c} \cdot 100 \tag{1}$$

where FR_s is the firing rate in response to a specific change, FR_c is the firing rate of the neuron in control (normocapnic) conditions (1.43 Hz), and Δs is the minimum increase or decrease of the signal necessary to produce an observable change in the firing rate. In other words, this value represents how much the neuron has to be stimulated with a particular signal in order to change its firing rate response from normal to altered activity. That is to say that in the case of chemical signals, a decrease in extracellular pH from 7.44 to 7.34, or an increase in the CO_2 level from 5% to 7%, is enough to produce an increased firing rate response (see Table 2).

Overall, the effect of applied stimulus current on the increased firing-rate response exceeds the contribution of chemical signals. According to calculated SI values, a small change in
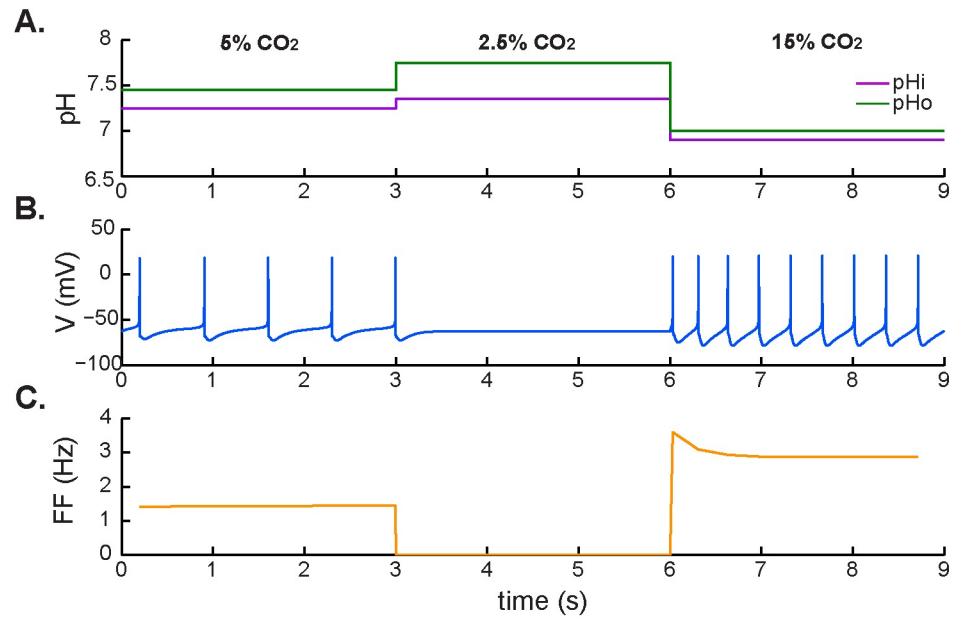
Fig 6. Neuronal response to hypocapnic and hypercapnic stimulation. A. Application of simulated normocapnia (5% CO_2), hypocapnic alkalosis (2.5% CO_2), and hypercapnic acidosis (15% CO_2). **B.** Corresponding membrane potential. **C.** Firing frequency during changing chemical conditions.

applied current (0.02 nA) can double the firing frequency, while a small reduction in pH (0.1 units) increases the firing rate by less than 42%. Small changes in %CO_2 constitute the signal for which the model results are less sensitive, causing an increase in firing rate of about 2%. This effect is schematized in Fig 7. Here, the firing-rate response increases indefinitely with injected depolarizing current (Fig 7C), but saturates for chemical stimuli (Fig 7A and 7B).

Fig 8 shows the effect of external stimuli on the simulated membrane potential of a spontaneously active neuron in response to different chemical stimuli and the firing frequency for a set of conditions (normocapnia, isohydric hypercapnia, isocapnic acidosis, or hypercapnic acidosis) at different values of the stimulus current. We observed the combined effect of the applied current and the chemical signals for three different stimulating external currents (I_s): depolarizing ($I_s < 0$), no electrical stimulus ($I_s = 0$), and hyperpolarizing ($I_s > 0$). From Fig 8B we noticed that whereas the firing frequency remained unchanged for acidotic conditions (i.e. IA and HA dark blue bars), it increased with excitatory input ($I_s = -0.6$) and decreased with inhibitory input ($I_s = 0.6$) at isohydric conditions (i.e. grey and light blue bars).

In addition, for each of the three acidotic conditions, we calculated the sensitivity of the firing rate at different stimulus currents using Eq 1 (see Table 3). Bars of the same color in Fig 8C

Table 2. Sensitivity of firing frequency to independent signals.

Signal	Control value	Δs	FR$_s$ (Hz)	Slope (Hz/[s])	SI (%)
I_s	0	0.02 nA	2.87	−71.9	100.7
CO_2	5%	2%	1.46	0.014	2.09
pH$_i$	7.25	0.1	1.78	−3.5	24.47
pH$_o$	7.45	0.1	2.02	−5.9	41.26

Sensitivity (SI) relative to signal, calculated for different signals. As in Eq (1), it is defined as the percentage of control firing rate (FR$_c$ = 1.43 Hz) to which firing rate increases or decreases in response to a change, Δs, in each signal. Signals: stimulus current (I_s), carbon dioxide level (CO_2), intracellular pH (pH$_i$), extracellular pH (pH$_o$).
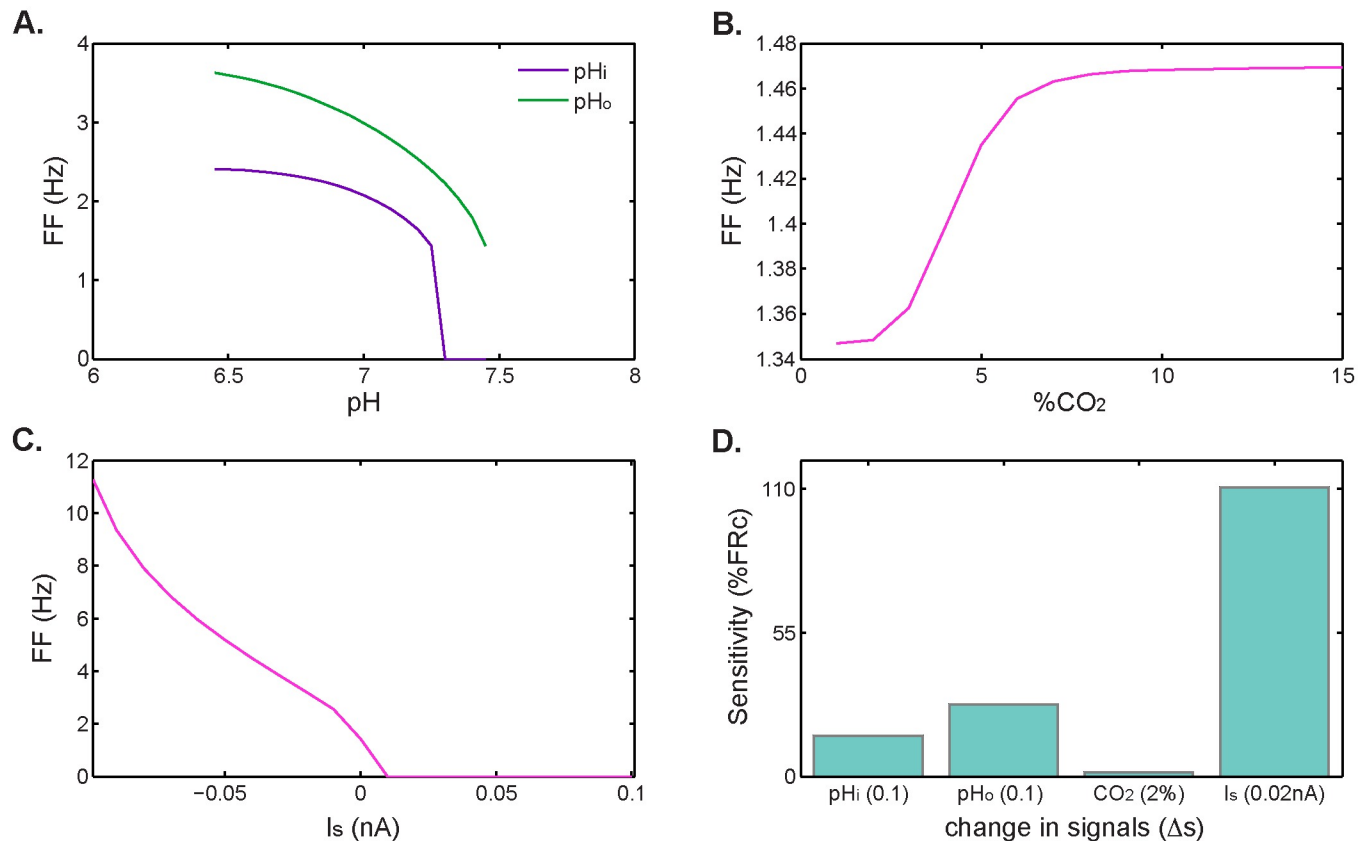
Fig 7. Effect of electrical and chemical signals on firing rate. A. Firing frequencies at different extracellular and intracellular pH levels, **B.** Firing frequency for different levels of CO_2. **C.** Firing frequency for different external stimulus current values (negative values for depolarizing current. **D.** Contribution of each signal to the firing-rate response measured as the percentage change from control firing rate upon exposure to each signal.

represent the sensitivity of the firing-rate response to the same chemical condition but at different stimulus currents. In general, Fig 8C shows that the sensitivity of the model in each case increases with inhibitory input, as a consequence of an increase in the difference in firing rate between control (dark grey) and acidotic/hypercapnic conditions (blue bars), as can be also observed from Fig 8B.

Discussion

We have developed a computational model of a spontaneously active single-neuron composed of CO_2/H^+-sensitive currents that reproduces the typical electrochemical behavior of individual brainstem neurons. The neuronal behaviors it describes have been observed both in computational models of neurons from different medullary regions and in experimental studies from brainstem chemosensitive nuclei [11,22,25,27]. The model specifically reproduces the regular pacemaker-like spiking pattern, action potential shape, and most of the membrane properties that characterize CO_2/H^+-sensitive neurons of the locus coeruleus.

Neurocomputational aspects

Modulation of spike frequency is a fundamental intrinsic property regulating repetitive firing dynamics in response to constant stimuli. Our results demonstrate that during the stimulation, in response to an external current or an excitatory chemical stimulus, there is an adaptation of
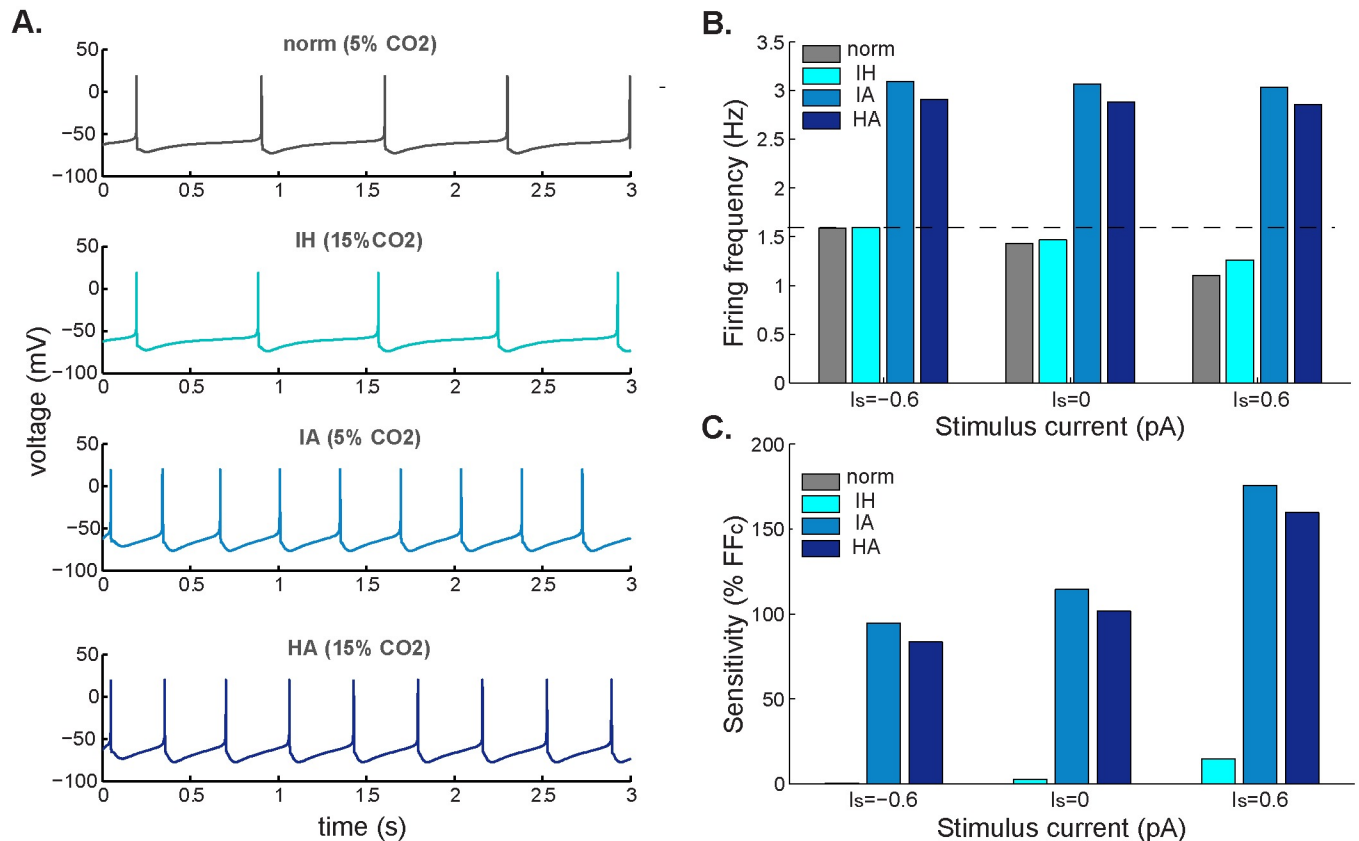
Fig 8. Firing frequency response to different electrical and chemical stimuli. A. Simulated membrane potential for different chemical stimuli: control (normocapnic: 5% CO_2, pH_o = 7.45, pH_i = 7.25), isohydric hypercapnia (IH: 15% CO_2, pH_o = 7.45, pH_i = 7.25), isocapnic acidosis (IA: 5% CO_2, pH_o = 7.1, pH_i = 7.0), and hypercapnic acidosis (HA: 15% CO_2, pH_o = 7.1, pH_i = 7.0). **B.** Firing rate under normocapnia (grey bar) and the same chemical stimuli as in A (blue bars) at different values of external applied current: excitatory stimulus current, I_s < 0; spontaneously firing neuron, I_s = 0; and inhibitory stimulus current, I_s > 0. **C.** Sensitivity for each chemical stimulus was calculated as the percentage increase from control firing rate.

the firing rate that regulates the initial activity in response to depolarization (Figs 1 and 2). Results from previous studies in chemosensitive brainstem regions suggest that such modulation of the action potential frequency is determined by the amplitude of the afterhyperpolarization phase of the action potential, which can be triggered by the inactivation of Ca^{2+}-activated K^+ currents [29,31].

Table 3. Sensitivity of firing frequency to different chemical stimuli.

Stimulus	pH_o	pH_i	%CO_2	FR_s	SI (%)
N	7.45	7.25	5	1.43	0
IH	7.45	7.25	15	1.26	11.9
IA	7.10	7.00	5	3.03	111.9
HA	7.10	7.00	15	2.85	99.3
HA*	7.10	7.25	15	2.68	87.4

The sensitivity (SI) is relative to the stimulus and is calculated for different chemical conditions. As in Eq (1), it is defined as the percentage of control firing rate (FR_c = 1.43 Hz) to which the firing rate changes (FR_s) in response to a specific chemical stimulus. Stimuli: normocapnia (N), isohydric hypercapnia (IH), isocapnic acidosis (IA), hypercapnic acidosis (HA), hypercapnic acidosis with no change in intracellular pH (HA*).

In agreement with previous studies, our results suggest that the mechanism of decay of the firing frequency responsible for SFA (Figs 2 and 3) and post-stimulation rebound (Fig 4C) involves an increase in calcium ion concentration inside the cell during depolarization. This accumulation of Ca^{2+} strengthens a calcium-activated K^+ current (in this case the SK current) that transiently diminishes the initial firing rate (Fig 2D and 2E). The same mechanism was observed upon termination of the rebound in Fig 4C, where the level of $[Ca^{2+}]_i$ gradually started to decay. In both cases, once resting levels of $[Ca^{2+}]_i$ had been restored, spiking resumed at an increased steady-state rate.

In addition, we found that the modulation of the firing frequency during electrical stimulation was not only associated with intracellular calcium accumulation and corresponding SK current activation (Fig 2C and 2D), but also with an inhibitory effect of the M-type K^+ current (Fig 2A–2C). In fact, there was less adaptation during chemical stimulation (reflected by a lower SFA value) where the M-type K^+ current played no role. From these results, we propose that the M-type current plays a major role in modulating a high peak frequency during electrical stimulation and that the calcium-activated mechanism responsible for adaptation plays a more important role during chemical stimulation.

Previous studies on respiratory neurons suggest that the T-type calcium current is the main current responsible for the initiation and evolution of the postinhibitory rebound that results when the neuron is released from the hyperpolarizing stimulus followed by stimulation with a depolarizing pulse. In agreement with Rybak [32], we found that the dynamic response of the membrane potential under these conditions is associated with an increase in T-type Ca^{2+} current, which depolarizes the membrane and promotes accumulation of intracellular calcium. There is also an increase in A-type current that may limit the rebound spiking frequency (Fig 4B). In the same way, T-type current activation is associated with the initial depolarization that causes the rebound of action potentials and modulates its frequency as it decreases to its initial state.

During external electrical stimulation we also observed delayed excitation after the rebound (Fig 4C) due to a weaker activation of the SK current. In contrast with this response to depolarizing and hyperpolarizing external stimuli, there was no evidence of delayed excitation–not even a depolarizing sag was seen–when stimulation was based only on physiological CO_2/H^+ changes (Fig 6). This is in accordance with findings from a model of central CO_2 chemosensitivity in *Helix aspersa* [44], which postulates that the A-type K+ current is the primary sensor for chemosensitive response to hypercapnic acidosis. However, we found that it is the M-type, not the A-type, K+ current that is most involved initiating the increased firing-rate response when stimulated with external input. In any case, we have no evidence from the present study that the M-type or pH-sensitive A-type potassium currents initiate the chemosensitive response to hypercapnic excitation, although Li & Putnam (2013) show a major role for A-currents in the hypercapnic response of locus coeruleus neurons [45].

Chemosensitive behavior

There are two interesting findings from the model. First, the increased firing-rate response to excitatory stimuli seems to saturate at increasing levels of CO_2 and/or acidification. This is in accordance with previous observations from the locus coeruleus, where a saturation effect seems to govern the neuron's chemosensitive behavior [46]. Second, a higher chemosensitivity is obtained with this model when the chemical stimulus involves decreased intracellular and extracellular pH but not an increase in CO_2 level alone. It can be seen from the relatively high value of the SI calculated for the increased firing rate in isocapnic acidosis. This observation is

also strengthened by the relatively low value of SI that was obtained in isohydric hypercapnia, when the stimulus involved an increase in CO_2 but the pH remained at the control level.

The fact that extracellular and not intracellular pH plays the major role in chemical signaling (Fig 7D) disagrees with a study by Filosa et al. (2002), in which the increased firing rate of locus coeruleus neurons in response to acid challenges correlated most with the magnitude and the rate of fall in pH_i [47]. This discrepancy can be explained in part because of the indirect limiting effect that pH_o has in the model. In other words, pH_o has the potential to inhibit the L-type calcium current, thus preventing the activation of the calcium-activated braking pathway and ultimately increasing the firing-rate response to acidotic challenges.

Indeed, the indirect effect that chemical signals may exert on the model's response to hypercapnic acidosis constitutes an important limitation of the model. We assumed an additive effect of signals on membrane protein activity, but it is clear that there is an intricate interaction between activated and inhibited currents. For example, acid inhibition of a K^+ channel could depolarize the membrane, which itself may activate another K^+ current, thus reducing the initial depolarizing effect of the pH-sensitive channel. This interaction, and many others, makes the precise combined effect of different signals difficult to predict. However, the assumption of separate and additive effects of signals on membrane protein activity is supported by the previous observation that contributions of each current to the overall effect of hypercapnic acidosis are approximately additive [48].

Importantly, the present work confirms that small external electrical signals play a greater role in determining the chemosensitive response to changes in CO_2/H^+ than previously thought. This implies that a neuron can be erroneously classified experimentally as a chemosensitive or non-chemosensitive cell if external electrical factors (e.g. input resistance or gap junctions) are not properly blocked. Furthermore, this observation supports the notion that synaptic transmission is very likely to modulate the responses of chemosensitive neurons [48], and highlights the importance of considering synaptic transmission when defining and understanding key concepts such as intrinsic chemosensitivity.

Model

The ionic current model describing neuronal activity is based on the Hodgkin–Huxley formalism, with membrane potential V and dynamics described as

$$c\frac{dV}{dt} = \sum_i I_i + I_s, \ \ i \in \{\text{Na, K}_{dr}, \text{K}_{ir}, \text{K}_A, \text{K}_M, \text{H, Ca}_L, \text{Ca}_N, \text{Ca}_T, \text{BK, SK, B}\} \quad (2)$$

where c is the neuron membrane capacitance (nF), I_s is a stimulus current (nA), representing an external stimulus coming from different sources (i.e. chemical synapses, gap junctions, injected currents, etc.) and I_i (nA) is the current flowing through the membrane channel i.

To propose a minimal configuration of an LC chemosensitive neuron the model incorporates different kinds of ion channels that have been identified in this nucleus, some of them known to play an important role in the intrinsic chemosensitive response of individual neurons. This set of membrane ionic currents consists of: transient sodium (Na) [29], delayed and inward rectifier potassium (Kir, Kdr) [24,43,45,50], transient potassium (K_A, K_M) [45,49], low and high threshold calcium (Ca_L, Ca_T) [18,51], calcium-dependent potassium channels (K_{BK}, K_{SK}) [19,29], and hyperpolarization-activated cation current [52]. We also included a background current (B) that accounted for the activity of non-selective leak potassium channels [53], and Na^+/Cl^- currents flowing throughout the membrane owing to the action of intracellular pH-regulating transporters [29].

For voltage-dependent channels, each flowing current is expressed as

Table 4. Cell properties and ionic equilibrium potentials.

Cell Properties			Nernst Potentials (mV)	
V_r	[mV]	−60	E_K	−93
R_{in}	[MΩ]	241.5	E_H	−45
A	[mm²]	4	E_{Ca}	60
c	[nF]	0.04	E_{Cl}	−93
I_s	[nA]	0	E_{Na}	45

These biophysical properties are from a typical rat raphe neuron and were taken from refs [42] and [51]. V_r: resting membrane voltage; R_{in}: input resistance; A: total area including soma and dendrites; c: capacitance (estimated from A, using the 1 µF/cm² rule); E_i: Nernst or equilibrium potentials for the ion species. The external stimulus current, I_s, was set to 0 to account for intrinsic neuronal response (e.g. spontaneous activity without external stimuli).

https://doi.org/10.1371/journal.pcbi.1005853.t004

$$I_i = g_i(E_i - V) \tag{3}$$

where g_i (µS) is the conductance of channel i, and E_i (mV) is its equilibrium reversal potential (Table 4). The conductance associated with each channel is represented as

$$g_i = \varphi_i \bar{g}_i m_i^{\alpha_i} h_i^{\beta_i} \tag{4}$$

where $\bar{g}_i$ is the maximal conductance of the i channel with activation and inactivation variables m_i and h_i, respectively (Table 5). φ_i, $0 < \varphi_i < 1$ is a scaling factor that modulates the magnitude of the currents to account for the CO_2/H^+ sensitivity of the channels.

The general formulation for the kinetics of ionic channels is based on previous brainstem single-neuron models [15,36]. Here, expressions for H^+/CO_2 sensitivity were included to each channel to account for chemosensory function and the resulting expressions were later fitted to experimental data in LC. Given the variability among identified neurons from LC, parameter values were optimized by eye, integrating the model for the appropriate current to fit individual currents under conditions that simulated normocapnic or hypercapnic acidotic experiments.

Activation and inactivation dynamics

The rates of activation and inactivation for voltage-sensitive channels are defined as first-order differential equations of the general form:

$$\frac{dx}{dt} = \frac{x^\infty - x}{\tau_x}, \; x \in \{m_i, h_i\} \tag{5}$$

Table 5. Maximal conductance for ionic currents.

Inward currents	Conductance (µS)	Outward currents	Conductance (µS)
Na	0.5940	K_{dr}	0.0384
H	0.0180	K_M	0.0005
Ca_T	0.1126	K_A	1.5
Ca_L	0.0005	SK	0.0030
Ca_L	0.0005	TASK	0.002

This set of values for maximal conductance yielded regular spontaneous activity ($I_s = 0$) and were adapted from ref [42]. Maximal conductance for the TASK potassium current was set at 0.002 µS, which is in the range reported in ref [53]. Abbreviations for currents as in Eq 2.

https://doi.org/10.1371/journal.pcbi.1005853.t005

with steady-state values x^∞

$$x^\infty = \frac{1}{1 + e^{-(V-V_x)/k_x}},$$ (6)

where V_x and k_x are half-activation voltage and slope factor, respectively (Tables 6 and 7). For each activation/inactivation variable x, time constant is defined by:

$$\tau_x = \begin{cases} a_x + b_x e^{-((V-V_{\tau_x})/k_{\tau_x})^2} & if\ x \in \{m_{Na}, h_{Na}, h_T\} \\ a_x + \dfrac{b_x}{cosh((V - V_{\tau_x})/k_{\tau_x})} & otherwise \end{cases}$$ (7)

CO$_2$/H$^+$ sensitivity

We used the Hodgkin–Huxley formalism as a basis to include the effect of CO_2 and H^+ on the neuronal response. We implemented neuronal chemosensitivity in this ionic current model by quantifying the total CO_2/H^+ sensitivity of each channel and considering the excitatory and inhibitory role that hypercapnic and/or acidotic stimuli would have on individual channels due to the combined effect of independent signals.

To approximate the total sensitivity of each channel, we assumed separate and additive effects of signals on membrane protein activity [22]. Thus, we expressed CO_2/H^+ sensitivity as a unitless function ($\varphi_i > 0$):

$$\varphi_i = 1 - \sum_s w_{i,s}\varphi_{i,s}, \quad s \in \{pH_o, pH_i, CO_2\}$$ (8)

where $\varphi_{i,s}$ defines specific functions for pH-dependent inhibition/activation of the channel i, and $w_{i,s}$ is the contribution of the signal, s (extracellular pH, intracellular pH and/or CO_2), to the present level of chemosensitivity. Here, a negative $w_{i,s}$ accounts for channel activation and a positive value for inhibition. For non-chemosensitive currents, the contribution of $w_{i,s}$ is set to zero (see Table 8).

In accordance with [54], we assumed that pH sensitivity (due to changes in pH_o or pH_i) relies on titrable amino acid residues in the channel protein. In the case of CO_2-dependent activation, CO_2 molecules are supposed to bind the channels and promote a second open state that enhances its activity [55]. As both situations describe a typical saturation effect, we express the relation between each signal and current inhibition/activation as a Hill equation:

$$\varphi_{i,s}(s) = \frac{1}{1 + (s_{1/2}/s)^{h_s}}$$ (9)

Table 6. Activation dynamics variables.

Par./current	units	Na	K$_{dr}$	K$_M$	K$_A$	Ca$_T$	Ca$_L$	Ca$_N$	BK	I$_H$
α		3	1	1	4	2	2	2	1	1
V$_m$	(mV)	-34.77	-15	-30	-57	-54.15	-20	-10	-20	-80
k$_m$		10.5	7	9	8.5	6.2	8.4	7	2	5
a$_m$		0.05	1	100	0.37	0.7	0.5	1	2	900
b$_m$		0.15	4	0	2	13.5	1.5	1.5	0	---
V$_{\tau m}$	(mV)	-43	-20	---	-55	-76	-20	-15	---	-80

Activation parameters for each current: number of gates, α_i, half-activation voltage, V$_m$, activation slope factor, k$_m$, and specific parameters for the time constant function a$_m$, b$_m$, V$_{\tau m}$. These values were taken from ref [42]. Where no unit is specified, parameters are unit-less values. Abbreviations for currents are as in Eq 2.

Table 7. Inactivation dynamics variables.

Par./current	units	Na	K_{dr}	K_M	K_A	Ca_T	Ca_L	Ca_N	BK	I_H
V_h	(mV)	-50.3	-78	-81	-45	-45	-50.3	-78	-81	-45
K_h		6.5	6	4	13.8	10	6.5	6	4	13.8
a_h		0.5	19	28	200	1000	0.5	19	28	200
b_h		7.5	45	300	0	0	7.5	45	300	0
$V_{\tau h}$	(mV)	-43	-80	-81	---	---	-43	-80	-81	---

Inactivation parameter values for each current: half-inactivation voltage, V_h, inactivation slope factor, k_h, and specific parameters for inactivation time constant function a_h, b_h, $V_{\tau h}$. These values were taken from ref [42]. Where no unit is specified, parameters are unit-less values. Abbreviations for currents as in Eq 2.

where $s_{1/2}$ corresponds either to the pK (pH level at the midpoint of current inhibition) or to the percentage of CO_2 required to achieve a half-maximal activation (Table 9). Hill coefficients h_s for each curve represent the sensitivity to each stimulus. Parameter values for intracellular and extracellular pH responses (titration curves) are shown in Table 10.

Calcium dynamics and Ca^{2+}-activated currents

Calcium-activated currents. Following ref [42] we assumed no explicit inactivation process for SK currents as its decay depends only on $[Ca^{2+}]_i$. We used a calcium-dependent steady-state activation variable for the SK current:

$$m_{SK}^{\infty} = \frac{Ca_{in}^n}{Ca_{in}^n - K_c^n} \tag{10}$$

where n is the Hill coefficient and K_c is the value of Ca_{in} at half-activation for m_{SK}^{∞} (Table 11). A recent study of firing activity on raphe neurons provided a more accurate estimate of the big potassium channel (BK) current by using a simplified model, in which, instead of considering the Ca^{2+} dependence of the BK channel conductance, it was coupled with N-type Ca^{2+} [42]. As there is evidence that BK channels are linked to L-type voltage-gated calcium currents in the rat brain [56], we used the Ca^{2+} current-coupled BK model for this current. The BK conductance was therefore coupled to the L-type Ca^{2+} channel, so the current was expressed as

$$I_{BK} = g_{BK} L (E_i - V) \tag{11}$$

where L is a unitless value representing the magnitude of the L-type Ca^{2+} current.

Calcium ion dynamics. The dynamics of free Ca^{2+} are assumed to occur inside a thin shell volume v, determined by the thickness and total area of the cell (see Table 4). Free calcium ions outside the neuron flow into it through voltage-gated Ca^{2+} channels and are then

Table 8. Contribution of chemical signals to CO_2/H^+ sensitivity in each channel.

weight/current	K_A	K_{dr}	K_{ir}	Ca_T	Ca_L	BK	K_{Leak}
w_{pHi}	0.3	1	1	0	0	1	0.5
w_{pHo}	0.7	0	0	1	0.3	0	0.5
w_{CO2}	0	0	0	0	0.7	0	0

Channel-specific weights assigned to each signal. Intracellular pH, w_{pHi}, extracellular pH, w_{pH0}, and CO_2 level, w_{CO2}. For non-chemosensitive currents the weight is set to zero. These values were adjusted to fit percentage of activation/inactivation of specific currents in different acidotic challenges [23,45,47,49]. Abbreviations for currents as in Eq 2.

Table 9. Signal values at midpoint current inhibition/or activation.

$S_{1/2}$/current	K_A	K_{dr}	K_{ir}	Ca_T	Ca_L	BK	K_{Leak}
pK_i	7.4	7.1	7	---	---	6.5	7.3
pK_o	7.3	---	---	6.9	6.5	---	7.4
$(CO_2)_{1/2}$	---	---	---	---	5	---	---

Midpoint values for current inhibition/activation curves. A pK value was assigned to intracellular (pK_i) and extracellular (pK_o) pH titration curves. The percentage of CO_2 required to achieve half-maximal current activation, $(CO2)_{1/2}$ was calculated as an approximation to fit data from ref [19]. Abbreviations for currents as in Eq 2.

https://doi.org/10.1371/journal.pcbi.1005853.t009

buffered or pumped out of the neuron by membrane transporters like the plasma membrane Ca^{2+} ATPase pump. Thus, $[Ca^{2+}]_i$ dynamics can be described by the following differential equation:

$$\frac{dCa_{in}}{dt} = \frac{-\text{CSF}(I_{Ca})}{2Fv} \cdot (1 - P_B) - K_s \frac{Ca_{in}}{Ca_{in} + K_m} \quad (12)$$

where v is the volume of a thin shell just inside the membrane and F is the Faraday constant, and I_{Ca} represents the sum of high-threshold calcium currents. We included a calcium source factor (CSF; $0 < \text{CSF} < 1$) that, where necessary, regulates the extent to which the internal calcium ion concentration is due to the calcium ions flowing through the currents [42]. The last (Michaelis–Menten) expression in the above equation is used to describe the pump mechanisms that maintain a low $[Ca^{2+}]_i$, where K_s is the maximal pumping rate and K_m is the dissociation constant ($[Ca^{2+}]_i$ for half-maximal rate). The bound fraction of Ca^{2+}, P_B, is given by

$$P_B = \frac{B_{tot}}{Ca_{in} + B_{tot} + K_d} \quad (13)$$

with B_{tot} representing the sum of the free and bound buffer and K_d being the dissociation constant of the reversible reaction underlying the binding of buffer B to Ca^{2+}. These models for BK channel and Ca^{2+} dynamics are described in [42] and the parameter values are listed in Table 11.

Background currents

CO_2/H^+-dependent inward rectification has been observed in adult and neonatal rat neurons from various chemosensitive regions. We therefore included an inwardly rectifying current

Table 10. Hill coefficients for titration/saturation curves.

Hill constant/current	K_A	K_{dr}	K_{ir}	Ca_T	Ca_L	BK	K_{leak}
h_i	15	15	15	---	---	2	1
h_o	15	0	---	1	1	---	---
h_c	---	---	---	---	5	---	---

Hill coefficient values for current's titration curve(s). Hill values in the table were calculated by fitting reported titration curves that allowed specific % change in ionic currents when different acidotic challenges were applied [23,45,47,49]. h_i for changing intracellular pH, h_o for changing extracellular pH, and h_c for changing CO_2 level. Abbreviations for currents as in Eq 2.

https://doi.org/10.1371/journal.pcbi.1005853.t010

Table 11. Calcium dynamics and SK parameter values.

Ca dynamics parameters			SK activation parameters		
K_d	(mM)	0.001			
CFS	---	0.201	Ca_{in}	(nM)	50
F	(Cmol^{-1})	96500	n	---	2
d	(μm^2)	0.062	K_c	(mM)	25
v	(mm^3)	0.25	α	---	1
K_s	(nMs^{-1})	0.390625	a_m	(ms)	5
K_m	(mM)	0.0001	b_m	(ms)	0
B_{tot}	(mM)	0.03			

These values were taken from [42]. The shell volume v was calculated as the total area of the neuron × shell thickness (Table 4). Abbreviations for Ca dynamics as in Eqs 12 and 13. Parameter values for BK activation: α_i, is the number of activation gates, and a_m, b_m are specific parameters for the time constant function (Eq 7). Other abbreviations for BK activation as in Eq 10.

(I_{Kir}), with a reversal potential of −44 mV taken from [31]:

$$I_{K_{ir}} = \bar{g}_{K_{ir}} \frac{(V - E_K - 36)}{1 + exp\{(V - E_K + 140)ZF/RT\}} \tag{14}$$

Assuming that there is a non-zero ion flux at rest, as the neuron fires spontaneously without afferent input, we added a small background current stated to be composed of chloride, sodium and potassium. Our reason for including these leak currents is because intracellular pH regulation by acid–base transporters results in altered neuronal excitability and their effect might be brought about by the pH modulation of Na$^+$/H$^+$ and Cl$^-$/HCO^{3-} exchangers [57]. In addition, pH$_o$-sensitive K$^+$ leak currents like the TASK-1 channel are expressed in chemosensitive neurons [58] and seem to be involved in the chemosensitive response of these neurons to hypercapnia. As the resting membrane potential will also be affected by the action of these factors, this change can be modeled by the following approximate formula, which assumes that sodium and chloride ion flux, from pH$_i$-regulating proteins, balances leak K$^+$ flux:

$$I_B = \sum_j I_{j,leak} \qquad j \in \{Na, K, Cl\} \tag{15}$$

with different leak currents expressed as linear $I_{j,leak} = g_{j,leak}(V - E_j)$. As the total leak conductance can be estimated as the reciprocal of the neuron's input resistance we obtain:

$$g_{K,leak} = g_{task} \tag{16}$$

$$g_{Cl,leak} = g_{leak} - g_{K,leak} - g_{Na,leak} \tag{17}$$

$$g_{Na,leak} = \frac{(R_{in})^{-1}(E_{Cl} - V_r) + g_{K,leak}(E_{Cl} - E_K)}{E_{Cl} - E_{Na}} \tag{18}$$

where V_r is the membrane potential that gives an equivalent leak equilibrium potential around −65 mV [36] and R_{in} is the input resistance (Table 4).

The model was implemented in a MatLab programming environment using a variable-step differential equation solver. The resulting ODE system given by Eqs (2), (5) and (12) was solved numerically using the stiff variable-step differential equation solver ode15s. For each

simulation, the model was run until steady-state conditions, from which data and calculations were then collected.

Acknowledgments

Author Contributions

Conceptualization: Maria C. Quintero.

Data curation: Robert W. Putnam.

Formal analysis: Maria C. Quintero.

Funding acquisition: Maria C. Quintero.

Investigation: Maria C. Quintero, Robert W. Putnam.

Methodology: Maria C. Quintero.

Project administration: Maria C. Quintero, Juan M. Cordovez.

Resources: Maria C. Quintero, Robert W. Putnam, Juan M. Cordovez.

Software: Maria C. Quintero, Juan M. Cordovez.

Supervision: Robert W. Putnam, Juan M. Cordovez.

Validation: Maria C. Quintero, Robert W. Putnam.

Visualization: Maria C. Quintero.

Writing – original draft: Maria C. Quintero.

Writing – review & editing: Maria C. Quintero.

References

1. Nattie EE. Central chemosensitivity, sleep, and wakefulness. Respir Physiol. 2001 Dec; 129(1–2): 257–68. PMID: 11738659

2. Tresguerres M, Buck J, Levin LR. Physiological carbon dioxide, bicarbonate, and pH sensing. Pflugers Arch. 2010; 460(6): 953–64. https://doi.org/10.1007/s00424-010-0865-6 PMID: 20683624

3. Lahiri S, Forster RE. CO_2/H+ sensing: peripheral and central chemoreception. Int J Biochem Cell Biol. 2003; 35(10): 1413–35. PMID: 12818238

4. Nattie E, Li A. Central chemoreception is a complex system function that involves multiple brain stem sites. J Appl Physiol. 2009; 106(4): 1464–6. https://doi.org/10.1152/japplphysiol.00112.2008 PMID: 18467549

5. Nattie EE. CO_2, brainstem chemoreceptors and breathing. Prog Neurobiol. 1999; 59(4): 299–331. PMID: 10501632

6. Guyenet PG. The 2008 Carl Ludwig Lecture: retrotrapezoid nucleus, CO_2 homeostasis, and breathing automaticity. J Appl Physiol. 2008; 105(2): 404–16. https://doi.org/10.1152/japplphysiol.90452.2008 PMID: 18535135

7. Guyenet PG, Stornetta RL, Bayliss D a. Retrotrapezoid nucleus and central chemoreception. J Physiol. 2008; 586(8): 2043–8. https://doi.org/10.1113/jphysiol.2008.150870 PMID: 18308822

8. Guyenet P. How does CO_2 activate the neurons of the retrotrapezoid nucleus? J Physiol. 2012; 590 (10): 2183–4. https://doi.org/10.1113/jphysiol.2012.230466 PMID: 22589206

9. Nattie EE. The retrotrapezoid nucleus and the drive to breathe. J Physiol. 2006; 572(2): 311.

10. Richerson GB, Wang W, Hodges MR, Dohle CI, DiezaSampedro A. Homing in on the specific pheno-type(s) of central respiratory chemoreceptors. Exp. Physiol. 2005; 90(3): 259–66. https://doi.org/10.1113/expphysiol.2005.029843 PMID: 15728134

11. Moreira TS, Takakura AC, Damasceno RS, Falquetto B, Totola LT, Sobrinho CR, et al. Central chemo-receptors and neural mechanisms of cardiorespiratory control. Brazilian J Med Biol Res. 2011; 44(9): 883–9.

12. Feldman JL, Mitchell GS, Nattie EE. Breathing: Rhythmicity, Plasticity, Chemosensitivity. Annu Rev Neurosci. 2003; 26:239–66. https://doi.org/10.1146/annurev.neuro.26.041002.131103 PMID: 12598679

13. Alheid GF, McCrimmon DR. The chemical neuroanatomy of breathing. Respir Physiol Neurobiol. 2008; 164: 3–11. https://doi.org/10.1016/j.resp.2008.07.014 PMID: 18706532

14. Feldman JL, Del Negro CA, Gray PA. Understanding the rhythm of breathing: so near, yet so far. Annu Rev Physiol. 2013; 75: 423–52. https://doi.org/10.1146/annurev-physiol-040510-130049 PMID: 23121137

15. Darnall RA. The role of CO2 and central chemoreception in the control of breathing in the fetus and the neonate. Respir Physiol Neurobiol. 2010; 173(3): 201–12. https://doi.org/10.1016/j.resp.2010.04.009 PMID: 20399912

16. Shams H. Differential effects of CO2 and H+ as central stimuli of respiration in the cat. J Appl Physiol. 1985; 58(2): 357–64. PMID: 3920185

17. Hartzler LK, Dean JB, Putnam RW. The chemosensitive response of neurons from the locus coeruleus (LC) to hypercapnic acidosis with clamped intracellular pH. Adv Exp Med Biol. 2008; 605: 333–7. https://doi.org/10.1007/978-0-387-73693-8_58 PMID: 18085295

18. Putnam RW, Filosa JA, Ritucci NA. Cellular mechanisms involved in CO2 and acid signaling in chemo-sensitive neurons. Am J Physiol Cell Physiol. 2004; 287(6): C1493–C1526. https://doi.org/10.1152/ajpcell.00282.2004 PMID: 15525685

19. Imber AN, Santin JM, Graham CD, Putnam RW. A HCO3−dependent mechanism involving soluble adenylyl cyclase for the activation of Ca2+ currents in locus coeruleus neurons. Biochim Biophys Acta. 2015; 1842(1842): 2569–78.

20. Huckstepp R, Dale N. CO2 dependent opening of an inwardly rectifying K+ channel. Pflugers Arch a Eur J Physiol. 2011; 461:337–44.

21. Ritucci NA, Erlichman JS, Leiter JC, Putnam RW. The Response of Membrane Potential (Vm) and Intraccellular pH (pHi) to Hypercapnia in Neurons and Astrocytes from Rat Retrotrapezoid Nucleus (RTN). Am J Physiol Regul Integr Comp Physiol. 2006; 289(3): R851–R861.

22. Conrad SC, Nichols NL, Ritucci N a, Dean JB, Putnam RW. Development of chemosensitivity in neu-rons from the nucleus tractus solitarii (NTS) of neonatal rats. Respir Physiol Neurobiol. 2009; 166(1): 4–12. https://doi.org/10.1016/j.resp.2008.11.005 PMID: 19056522

23. Nichols NL, Mulkey DK, Wilkinson K a, Powell FL, Dean JB, Putnam RW. Characterization of the che-mosensitive response of individual solitary complex neurons from adult rats. Am J Physiol Regul Integr Comp Physiol. 2009; 296(3): R763–73. https://doi.org/10.1152/ajpregu.90769.2008 PMID: 19144749

24. Gargaglioni LH, Hartzler LK, Putnam RW. The locus coeruleus and central chemosensitivity. Respir Physiol Neurobiol. 2010; 173(3): 264–73. https://doi.org/10.1016/j.resp.2010.04.024 PMID: 20435170

25. Biancardi V, Bícego KC, Almeida MC, Gargaglioni LH. Locus coeruleus noradrenergic neurons and CO2 drive to breathing. Pflugers Arch. 2008; 455(6): 1119–28. https://doi.org/10.1007/s00424-007-0338-8 PMID: 17851683

26. Ritucci NA, Dean JB, Putnam RW. Somatic versus Dendritic Responses to Hypercapnia in Chemosen-sitive Locus Coeruleus Neurons from Neonatal Rats. Am J Physiol Cell Physiol. 2005; 289(5): C1094–C1104. https://doi.org/10.1152/ajpcell.00329.2004 PMID: 16014703

27. Corcoran AE, Hodges MR, Wu Y, Wang W, Wylie CJ, Deneris ES, et al. Medullary serotonin neurons and central CO2 chemoreception. Respir Physiol Neurobiol. 2009; 168(1–2): 49–58. https://doi.org/10.1016/j.resp.2009.04.014 PMID: 19394450

28. Putnam RW, Conrad SC, Gdovin MJ, Erlichman JS, Leiter JC. Neonatal maturation of the hypercapnic ventilatory response and central neural CO2 chemosensitivity. Respir Physiol Neurobiol. 2005; 149(1–3): 165–79. https://doi.org/10.1016/j.resp.2005.03.004 PMID: 15876557

29. Zhang X, Cui N, Wu Z, Su J, Tadepalli JS, Sekizar S, et al. Intrinsic membrane properties of locus coe-ruleus neurons in Mecp2anull mice. Am J Physiol Cell Physiol. 2010; 298(3):C635–46. https://doi.org/10.1152/ajpcell.00442.2009 PMID: 20042730

30. Athanasiades A, Clark JW, Ghorbel F, Bidani A. An ionic current model for medullary respiratory neu-rons. J Comput Neurosci. 2000; 9(3): 237–57. PMID: 11139041

31. Schild JH, Khushalani S, Clark JW, Andresen MC, Kunze DL, Yang M. An Ionic Current Model for Neu-rons in the Rat Medial Nucleus Tractus Solitarii Receiving Sensory Afferent Input. J Physiol. 1993; 469: 341–63. PMID: 7505824

32. Rybak IA, Paton JFR, Schwaber JS. Modeling Neural Mechanisms for Genesis of Respiratory Rhythm and Pattern. I. Models of Respiratory Neurons Modeling Neural Mechanisms for Genesis of Respiratory Rhythm and Pattern. I. Models of Respiratory Neurons. J Neurophysiol. 1997; 77: 1994–2006. PMID: 9114250

33. Rybak IA, Paton JFR, Schwaber JS, Orem JM, Solomon IC, Morris KF, et al. Modeling Neural Mechanisms for Genesis of Respiratory Rhythm and Pattern. II. Network Models of the Central Respiratory Pattern Generator. J Neurophysiol. 1997; 77: 2007–26. PMID: 9114251

34. Rubin JE, Bacak BJ, Molkov YI, Shevtsova NA, Smith JC, Rybak IA. Interacting oscillations in neural control of breathing: modeling and qualitative analysis. J Comput Neurosci. 2011; 30(3): 607–32. https://doi.org/10.1007/s10827-010-0281-0 PMID: 20927576

35. Molkov YI, Zoccal DB, Moraes DJA, Paton JFR, Machado BH, Rybak IA. Intermittent hypoxia induced sensitization of central chemoreceptors contributes to sympathetic nerve activity during late expiration in rats. J Neurophysiol. 2011; 1 05(6): 3080–91.

36. Horner RL, Bradley TD. Update in sleep and control of ventilation 2007. Am J Respir Crit Care Med. 2008; 1 77(9): 947–51.

37. Vollmer LL, Strawn JR, Sah R. Acid–base dysregulation and chemosensory mechanisms in panic disorder: a translational update. Transl Psychiatry. Nature Publishing Group; 2015; 5(e752): 1–11.

38. Kinkead R, Tenorio L, Drolet G, Bretzner F, Gargaglioni L. Respiratory manifestations of panic disorder in animals and humans: A unique opportunity to understand how supramedullary structures regulate breathing. Respir Physiol Neurobiol. 2014; 204: 3–13. https://doi.org/10.1016/j.resp.2014.06.013 PMID: 25038523

39. Sardinha A, Christophe R, Zin WA, Nardi AE. Respiratory manifestations of panic disorder: causes, consequences and therapeutic implications. J Bras Pneumol. 2009; 35(7): 698–708. PMID: 19669009

40. Wemmie JA. Neurobiology of panic and pH chemosensation in the brain. Dialogues Clin Neurosci. 2011; 1 3: 475–83.

41. Zhang X, Su J, Cui N, Gai H, Wu Z, Jiang C. The disruption of central CO_2 chemosensitivity in a mouse model of Rett syndrome. Am J Physiol Cell Physiol. 2011; 301(3): C729a38.

42. Tuckwell HC, Penington NJ. Computational modeling of spike generation in serotonergic neurons of the dorsal raphe nucleus. Prog Neurobiol. 2014; 118: 59–101. https://doi.org/10.1016/j.pneurobio.2014.04.001 PMID: 24784445

43. Williams JT, Marshall KC. Membrane properties and adrenergic responses in locus coeruleus neurons of young rats. J Neurosci. 1987; 7(11): 3687–94. PMID: 2890723

44. Chernov MM, Daubenspeck JA, Denton JS, Pfeiffer JR, Putnam RW, Leiter JC. A computational analysis of central CO_2 chemosensitivity in Helix aspersa. Am J Physiol Cell Physiol. 2007; 2 92(1): C278–91.

45. Li K, Putnam RW. Transient outwardly rectifying A currents are involved in the firing rate response to altered CO_2 in chemosensitive locus coeruleus neurons from neonatal rats. Am J Physiol Regul Integr Comp Physiol. 2013; 3 05(7): R780–R792.

46. Putnam RW. CO_2 chemoreception in cardiorespiratory control. J Appl Physiol. 2010; 108(6): 1796–802. https://doi.org/10.1152/japplphysiol.01169.2009 PMID: 20093663

47. Filosa JA, Dean JB, Putnam RW. Role of intracellular and extracellular pH in the chemosensitive response of rat locus coeruleus neurones. J Physiol. 2002; 541(2): 493–509.

48. Chernov M, Putnam RW, Leiter JC. A computer model of mammalian central CO_2 chemoreception. Adv Exp Med Biol. 2008; 605: 301–5. https://doi.org/10.1007/978-0-387-73693-8_52 PMID: 18085289

49. Li K, Putnam RW. Hypercapnia inhibits both transient and sustained potassium currents in chemosensitive neurons from neonatal rat locus coeruleus (LC). The FASEB Journal. p. 621.5.

50. Xu H, Cui N, Yang Z, Qu Z, Jiang C. Modulation of kir4.1 and kir5.1 by hypercapnia and intracellular acidosis. J Physiol. 2000; 524(3): 725–35.

51. Imber AN, Putnam RW. Postnatal development and activation of L-type Ca^{2+} currents in locus coeruleus neurons: implications for a role for Ca^{2+} in central chemosensitivity. J Appl Physiol. 2012; 1 12(10): 1715–26.

52. Santin JM, Hartzler LK. Activation state of the hyperpolarization activated current modulates temperature sensitivity of firing in locus coeruleus neurons from bullfrogs. Am J Physiol a Regul Integr Comp Physiol. 2015; 308(12): R1045–61.

53. Mulkey DK, Talley EM, Stornetta RL, Siegel AR, West GH, Chen X, et al. TASK channels determine pH sensitivity in select respiratory neurons but do not contribute to central respiratory chemosensitivity. J Neurosci. 2007; 2 7(51): 14049–58. Jiang C, Rojas A, Wang R, Wang X. CO_2 central chemosensitivity: why are there so many sensing molecules? Respir Physiol Neurobiol. 2005; 145: 115–26.

54. Huckstepp R, Dale N. Redefining the components of central CO2 chemosensitivity towards a better understanding of mechanism. J Physiol. 2011; 589(23): 5561–79.

55. Filosa JA, Putnam RW. Multiple targets of chemosensitive signaling in locus coeruleus neurons: role of K+ and Ca2+ channels. Am J Physiol Cell Physiol. 2003; 2 84: C145–55.

56. Weaver AK, Olsen ML, McFerrin MB, Sontheimer H. BK channels arelinked to inositol 1,4,5atriphosphate receptors via lipid rafts: a novel mechanism for coupling [Ca(2+)](i) to ion channel activation. J Biol Chem. 2007; 2 82(43): 31558–68.

57. Ruffin V a, Salameh AI, Boron WF, Parker MD. Intracellular pH regulation by acid base transporters in mammalian neurons. Front Physiol. 2014; 5(43): 1–11.

58. Bayliss DA, Talley EM, Sirois JE, Lei Q. TASKa1 is a highly modulated pHa sensitive leak K+ channel expressed in brainstem respiratory neurons. Respir Physiol. 2001; 1 29(1–2): 159–74.